Local Shell-Side Heat Transfer Coefficients and Pressure Drop in a Tubular Heat Exchanger with Orifice Baffles

K. S. LEE and J. G. KNUDSEN

Oregon State College, Corvallis, Oregon

By means of a moveable sensing probe previously described[2] local shell-side heat transfer coefficients and friction losses were measured on a model tubular heat exchanger containing orifice baffles. The heat exchanger shell was 6-in. nominal I.D. and 45 in. in length and contained four tubes in triangular arrangement passing through orifice baffles. Baffle hole diameters of 1-/16, 1-2/16, 1-3/16, and 1-5/16 in. and baffle spacings of 4.0 and 9.0 in. were studied. Data were taken at several air flow rates for each of the four baffle hole diameters.

The average heat transfer coefficient for the region between two central baffles was correlated with an empirical equation based on only two baffle spacings.

An increase in the baffle-to-tube clearance caused a decrease in heat transfer. An increase in the baffle spacing also resulted in a decrease in heat transfer. Four flow zones in the baffle space are postulated from the analysis of Nusselt number distribution along the tube. The heat transfer characteristics in each of the four flow zones were analyzed in terms of the mechanism of the fluid flow.

The pressure-drop data were correlated in terms of an annular orifice coefficient of discharge and an orifice-pressure-drop function. As a result of this study a method was developed by which one can predict the average of the local coefficients at the baffle position from the knowledge of pressure drop across a single baffle.

In a shell-and-tube baffled heat exchanger heat is transmitted from one moving fluid to another across the tube wall. Because of the complex flow patterns generally existing in the shell side of a baffled heat exchanger an accurate evaluation of the shell side heat transfer rate is one of the difficult aspects in the designing of such exchangers.

Considerable work has been directed toward the establishment of a rational correlation of the shell side heat transfer data. The best discussions available on this topic are those of Short (*8*) and Tinker (*10*). Short's work covers an extensive range of experimental data on various types of commercial units and correlates these data with a number of empirical equations. Tinker (*10*) proposed an improved method of correlation based on a more detailed analysis of shell side geometry and flow patterns. Sullivan and Bergelin (*9*) presented heat transfer and pressure-drop data for shell side flow around a single segmental baffle. A generalized method is presented to predict the pressure drop across the baffle with leakage through the baffle-to-tube clearances. The effect of leakage area upon heat transfer and pressure drop was discussed.

In an effort to obtain more basic information on the shell side heat transfer a program of research has been conducted. The previous workers in the program (*1, 2, 4*) indicated the need for a detailed study of regions close to the baffles, especially with regard to obtaining information on the effect of baffle-to-tube clearances on the shell side heat transfer.

For this purpose the present work has been conducted with a model heat exchanger containing orifice types of baffles in the shell. Local heat transfer coefficients were measured directly by the use of a sensing probe previously described (*1, 2, 4*), enabling one to measure the shell side heat transfer coefficient at any point in the heat exchanger.

EXPERIMENTAL EQUIPMENT

A schematic diagram of the experimental equipment is shown in Figure 1. It has been used by previous workers (*1, 2, 4*) in the study of segmentally baffled exchangers. Air is supplied by a Roots type of blower to the shell side of a model heat exchanger.

The model heat exchanger shell was fabricated from a cast lucite tube 45 in. long, 6-in. nominal diameter, and containing a tube bundle made up of four, 1-in. O.D. aluminum condenser tubes, steel tie rods, orifice baffles, and tube sheets. The orifice baffles were made from ⅛ in. thick lucite sheets. Each baffle had a diameter of 5.656 in. and four tube holes spaced at triangular pitch of 2-3/16 in. The tube-hole diameters were 1-1/16, 1-2/16, 1-3/16, and 1-5/16 in. (Figure 2). In Table 1 the dimensions of the major components of the model heat exchanger are given.

The sensing probe used to measure local heat transfer coefficients is the same as that used by previous workers (*1, 2, 4*). It consisted of a short section of 1-in. O.D. plastic tube mounted between two lengths of 1-in. O.D. aluminum tube. Three strips of 1-in. by 0.002-in. resistance ribbon were wrapped tightly around the plastic tube and connected in series. Power leads supplied DC power to the resistance ribbon. Seven iron-constantan thermocouples were placed under the central strip to measure surface temperatures of the ribbon. The location of the thermocouples is shown in Figure 2. This probe could be located along any tube position in the model heat exchanger.

K. S. Lee is at Carnegie Institute of Technology, Pittsburgh, Pennsylvania.

EXPERIMENTAL PROGRAM

The measurement of local heat transfer coefficients was restricted to the No. 1 tube at the uppermost position in the shell. The variables considered in this investigation were baffle-to-tube clearance (1/32, 1/16, 3/32, and 5/32 in.); baffle spacing (4-in. spacing with ten baffles in the exchanger, and 9-in. spacing with four baffles in the exchanger); and air flow rate through the exchanger. The range of flow rates for each baffle opening and spacing was determined by the permissible pressure drop for the equipment.

For the ten-baffle case the space between the No. 5 and No. 6 baffles was investigated at the baffles and at ¾-in. intervals between the baffles. For the four-baffle case the space between the No. 2 and No. 3 baffles was investigated at the baffles and at 1-in. intervals between the baffles. In the former ten positions and in the latter seven positions were investigated, seven circumferential local coefficients being determined at each position for each flow rate.

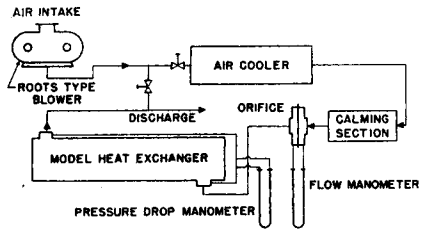

Fig. 1. Air flow system.

The experimental program is summarized in Table 2. [Original data obtained in this experiment are available (5).]

CALCULATIONS OF THE LOCAL HEAT TRANSFER COEFFICIENT

The local heat transfer coefficient may be determined from the amount of power supplied to the probe, the surface temperature at the probe, and the temperature of the flowing air (1, 2). An energy balance around a differential length of resistance ribbon results in a general expression for the local heat transfer coefficient, and when one neglects the radiation and conduction terms, the result is

$$h_s = \frac{11.10i^2 + 2{,}404\left(\frac{d^2t}{d\theta^2}\right)}{t - t_a} \quad (1)$$

Equation (1) was used to calculate the local heat transfer coefficients from the experimental measurements. The second derivative, $d^2t/d\theta^2$, was calculated numerically with a Milne three-point method (6).

ANALYSIS OF DATA

Average Shell Side Heat Transfer Data

All heat transfer data were first analyzed on the basis of average heat transfer coefficients in the baffle space so that the results could be compared with those of other workers who had measured only average shell side coefficients. In addition a preliminary correlation showing the effect of baffle spacing was attempted, even though only two baffle spacings were investigated.

The average shell side Nusselt number $(h_s D_1/k)_{av}$ was calculated in the following manner.

The local heat transfer coefficients at a tube cross section were averaged to obtain an arithmetic average coefficient at the section, which was then used to calculate the corresponding Nusselt number $(h_s D_1/k)$ at a cross section. These Nusselt numbers were plotted in their proper places along the tube length to obtain a Nusselt number distribution curve along the portion of the tube between two central baffles. The average Nusselt number $(h_s D_1/k)_{av}$ was calculated by integrating the curve and dividing the result by the distance between the two baffles. Mathematically expressed

$$\left(\frac{h_s D_1}{k}\right)_{av} = \frac{1}{L}\int_1^2 \left(\frac{h_s D_1}{k}\right) dL \quad (2)$$

The effect of baffle spacing is considered in the dimensionless ratio L/S (that is exchanger length/baffle spacing). It is conceivable that other length ratios may be used, but more baffle spacings should be studied in order to determine the best geometric ratio to use to account for the effect of baffle spacing. On the basis of the two baffle spacings studied it was found that the data could be correlated by plotting the dimensionless group

$$\left(\frac{h_s D_1}{k}\right)_{av}\left(\frac{c_p\mu}{k}\right)^{-1/3}\left(\frac{L}{S}\right)^{-0.35}$$

against the weighted shell side Reynolds number D_1G_e/μ as shown in Figure 3.

The Prandtl number of the air was taken as 0.7 in all cases. The weighted shell side Reynolds number D_1G_e/μ was based on a weighted shell side mass velocity G_e which was the geometric mean of the two mass velocities at two different flow areas, the flow area in a region between the baffles and the net flow area at the baffle; that is

$$G_e = \frac{w}{A_e} = \frac{w}{\sqrt{A_f A_b}} = \sqrt{G_f \cdot G_b} \quad (3)$$

Table 1. Dimensions of Model Heat Exchanger Components

Shell	
Inside diameter	5.72 ± 0.03 in.
Outside diameter	5.94 ± 0.03 in.
Length	45.0 in.
Baffles	
Baffle diameter	5.66 ± 0.03 in.
No. of baffle holes	4
Baffle hole diameters	1/16, 1-2/16, 1-3/16, 1-5/16 in.
Tube pitch	2-3/16 in.
Tubes	
Outside diameter	1.000 ± 0.001 in.
No. of tubes	4
Drilled Holes	
Tube holes in tube sheets	1.000 ± 0.003 in.
Tie-rod holes	3/16 in.
Flange-tube sheet bolt holes	1/4 in.

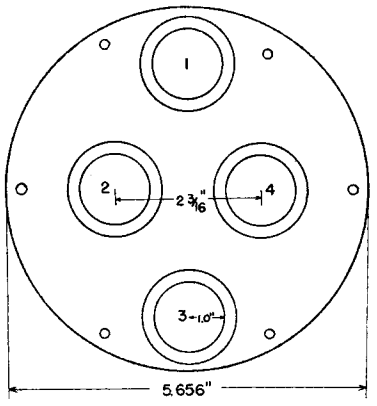

TUBES NUMBERED AT UP-STREAM END OF EXCHANGER

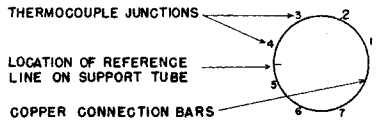

THERMOCOUPLES NUMBERED AT UP-STREAM END OF EXCHANGER

Fig. 2. Tube and thermocouple numbering system.

In Figure 3 all experimental data obtained fall on a single line. A residual summation analysis of the data resulted in the following empirical equation

$$\left(\frac{h_s D_1}{k}\right)_{av}\left(\frac{c_p\mu}{k}\right)^{-1/3} = 0.1625\left(\frac{D_1G_e}{\mu}\right)^{0.67}\left(\frac{L}{S}\right)^{0.35} \quad (4)$$

The average deviation of the data from Equation (4) is ± 3.5%.

The correlation developed here is satisfactory for the present data. Equation (4) is based on a limited amount

TABLE 2. SUMMARY OF EXPERIMENTAL DATA

No. of baffles	Baffle spacing, in.	Baffle-hole diameter, in.	Range of air flow rates, (cu. ft./min., 60°F, 1 atm.)	No. of coefficients measured
10	4.09	1-1/16	12-28	273
4	9.0	1-1/16	15-42	308
10	4.09	1-2/16	16-52	371
10	4.09	1-3/16	17-77	301
10	4.09	1-5/16	30-101	241
4	9.0	1-5/16	30-102	280

of data however, and further study is needed on other systems. The factor $(L/S)^{0.35}$, which accounts for the effect of the baffle spacing on the heat transfer rate, was based on the data on only two baffle spacings investigated. In addition the study of more baffle spacings should allow the determination of a better weighted mass velocity than the geometric mean that was used. The geometric mean assumes however that the heat transfer effects at the baffle and midway between the baffle are equal. An inspection of the Nusselt number distribution along the tube indicates that this assumption is not grossly in error.

The present data were also correlated according to one of Short's relationships based on data obtained from commercial orifice-baffled exchangers. The group

$$\left(\frac{h_o D_1}{k}\right)_{av} \left(\frac{c_p \mu}{k}\right)^{-0.32} \left(\frac{P}{P - D_1}\right)^{0.5}$$

is plotted vs. an average Reynolds number $(D_1 G_a/\mu)$ in Figure 4, and the result is compared with Short's results.

The mass velocity used in $(D_1 G_a/\mu)$ is defined as (8)

$$G_a = \left(\frac{L}{S}\right)^{0.55} \left[G_b \left(\frac{(D_2 - D_1) D_1}{P D_s} \right)^{0.88} + G_s \left(\frac{D_1^2}{A_s} \right)^{0.43} \right] \qquad (5)$$

The present data correlate well by this method but are approximately 100 to 120% higher than Short's results. A similar tendency was noted in Ambrose's work on segmental baffles (1, 2) when his data were compared with those of Short as reported by Donohue (3). Ambrose's data with a tube pitch of 2-3/16 in. were 100 to 150% higher than those reported by Donohue.

The generally high heat transfer coefficients for the model heat exchanger can be attributed to the following factors:

1. The tube pitch of 2-3/16 in. in the model heat exchanger was much greater than that of the commercial units tested by Short. The tube pitch used in Short's tests was between 11/16 and 1-1/16 in. and Short's correlation may not be valid at a tube pitch as large as 2-3/16 in. It has been found that larger tube pitches result in an increase in heat transfer rate (8).

2. The size of tubes in the present model heat exchanger was larger than that of others, which may have been another factor causing a high heat transfer rate.

3. The upstream portion of the sensing probe preceding the resistance ribbons was not heated. The presence of this unheated length gives a higher heat transfer rate at the resistance ribbon than would be true if the entire length were heated. Using Rubesin's (7) formula for a flat plate one could estimate the effect of the unheated length on heat transfer rate. The analysis indicated that for the 4-in. spacing one might expect the result obtained with the probe to be about 5.0% higher than when the whole tube is heated. For the 9.0-in. spacing the result might be expected to be about 10% higher.

4. The average shell side heat transfer coefficients reported by Short are based on a log mean temperature difference across the whole heat exchanger, while in the present work they are based on a true temperature difference. The extent to which the log mean temperature difference diverges from the true temperature difference could account for the lack of agreement between the two sets of data.

Heat Transfer at the Baffle Hole

The heat transfer rates at the baffle holes for both 4.0- and 9.0-in. baffle spacings are plotted in Figure 5, and the data correlated within ± 8.5% by the following equation:

$$\left(\frac{h_o D_1}{k}\right)_b \left(\frac{c_p \mu}{k}\right)^{-1/3} = 0.2388 \left(\frac{D_1}{D_e}\right)^{0.57} \left(\frac{D_e G_b}{\mu}\right)^{0.67} \qquad (6)$$

The Nusselt number at the baffle $(h_o D_1/k)_b$ is the arithmetic average of the two Nusselt numbers at each end of the baffle space studied. In most cases the Nusselt numbers at different baffle positions were close to each other, although in some cases considerable variation existed. The local coefficient is changing very rapidly with tube length, and a small error in position of the probe in the baffle hole could account for the large difference that occurs in a few instances.

In evaluating the Reynolds number at the baffle $(D_e G_b/\mu)$ the diameter is twice the clearance between baffle and the tube, $D_2 - D_1$. The mass velocity is the mass rate of flow divided by the total flow area available at the baffle; that is $G_b = (w/A_b)$.

The equivalent diameter of the annular orifice based on heated surface is $(D_2^2 - D_1^2)/D_1$. An attempt was made to correlate the data by using a Reynolds number based on this equivalent diameter. A better correlation was obtained however with D_e (twice the clearance between the tube and baffle) in the Reynolds number.

For the baffle spacings studied in the present work the heat transfer rates at the annular clearances between the baffle and tubes are independent of baffle spacing and are dependent only on the size of the baffle openings and flow rate. This conclusion is reasonable because the flow conditions in the annular clearance between the tube and the baffle are not expected to be af-

TABLE 3. APPROXIMATE LENGTHS OF FLOW ZONES

A. 10 Baffles (4.0-in. spacing)

Baffle hole diam., (in.)	Flow rate, (cu. ft./min.)	Zone A, (in.)	Zone B, (in.)	Zone C, (in.)	Zone D, (in.)
1-1/16	15-30	*	3.5	0	0.5
1-2/16	15-50	0.5	3.0	0	0.5
1-3/16	15-75	0.75	2.75	0	0.5
1-5/16	30-100	1.00	2.50	0	0.5
		B. 4 Baffles (9.0-in. spacing)			
1-1/16	25-42	*	4.0	4.5	0.5
1-5/16	30-100	1.0	3.0	4.5	0.5

* Length could not be determined from data obtained.

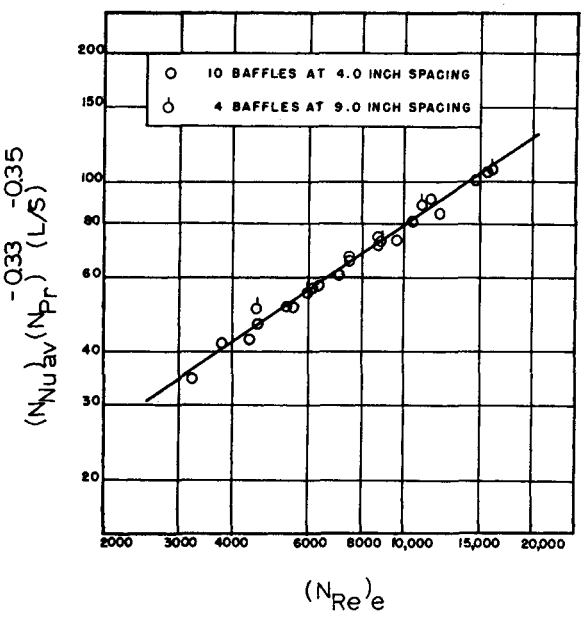

Fig. 3. Correlation of shell-side heat transfer data.

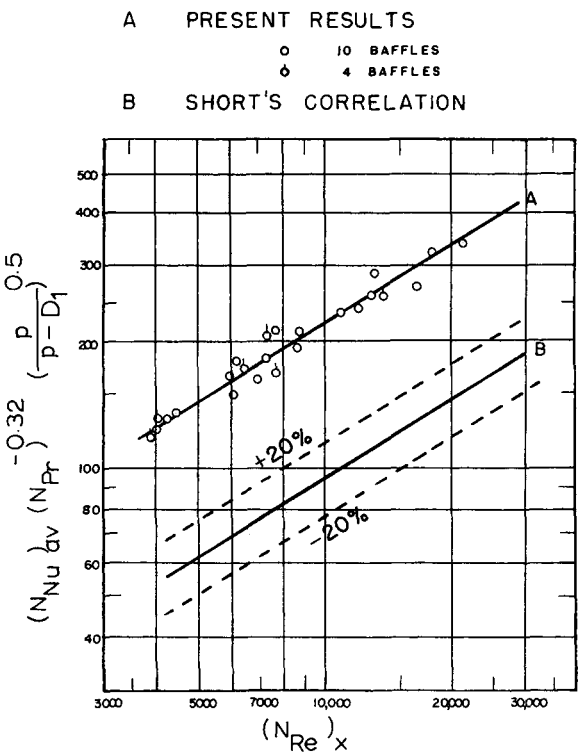

Fig. 4. Correlation of average heat transfer data.

fected by the baffle spacing, except perhaps when the baffles become very close together.

By the use of Equation (6) in conjunction with the orifice-pressure-drop function developed subsequently one can predict the average value of local heat transfer coefficients at the annular clearances formed between a baffle and tubes.

Flow Patterns and Nusselt Number Distribution Along the Tube

The flow pattern existing in the region between two adjacent orifice baffles is less complicated than that for segmental baffles. Short (8) pointed out that the shell side flow with orifice baffles was roughly parallel to the tubes. In the present work a more detailed flow pattern is postulated based upon the local Nusselt number distribution along the tube. In Figure 6 the average Nusselt numbers $(h_s D_1/k)$ at each cross section studied are plotted along the length of the tube for the ten-baffle spacing, 1-1/16- and 1-2/16-in. baffle holes, and in Figure 7 for the four-baffle spacing 1-1/16- and 1-5/16-in. holes. The average height of these curves gives $(h_s D_1/k)_{av}$ as defined in Equation (2). The points plotted in Figures 6 and 7 are joined by straight-line segments to show the variation of Nusselt number with length. Many more points would have to be investigated before a smooth curve could be drawn to accurately represent the variation with length.

Some interesting features are discernible however concerning the Nusselt number variation along the tube. High coefficients exist at the baffle hole. At the larger openings however a maximum in the heat transfer coefficient is evident, the position of this maximum being further from the baffle as the opening gets larger. The maximum also may exist for smaller openings but was not detected because the positions investigated were too far apart. Beyond the maximum the local rate of heat transfer decreases rapidly, passes through a minimum, and then increases abruptly just before the downstream baffle.

In order to render some quantitative interpretations to the curves in Figures 6 and 7, the following flow zones are defined:

Zone A starts at the upstream baffle and extends to a point where the Nusselt number assumes a maximum.

Zone B follows Zone A from the point of maximum Nusselt number and extends to a point where the Nusselt number reaches a minimum.

Zone C follows Zone B and extends to a point close to the downstream baffle. The criterion for this zone is that the local Nusselt number remains fairly constant, maintaining the minimum value attained at the end of Zone B.

Zone D is the remaining narrow region between the end of Zone C and the downstream baffle.

In Table 3 the approximate lengths of the flow zones defined above are tabulated at various flow rates and baffle-to-tube clearances. These lengths are only approximate since positions investigated are quite far apart.

At the beginning of Zone A the fluid is emerging from the small annular opening between the tube and baffle and consequently has a high velocity. This is evidenced by high heat transfer coefficients in this zone. The existence of a maximum value of the Nusselt number at the end of Zone A is probably due to the existence of eddies beyond the baffle caused by the jetting action of the flow through the orifice. The absence of a maximum with the 1-1/16-in. opening is presumably because the points investigated were too far apart.

In Zone B the local Nusselt number decreases steadily until it attains a minimum value. In this region a boundary layer builds up on the tubes, be-

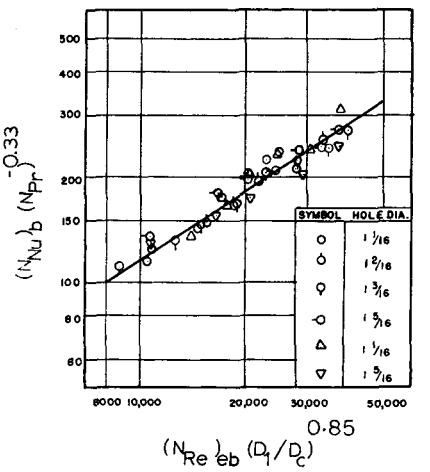

Fig. 5. Correlation of shell-side heat transfer data at baffles.

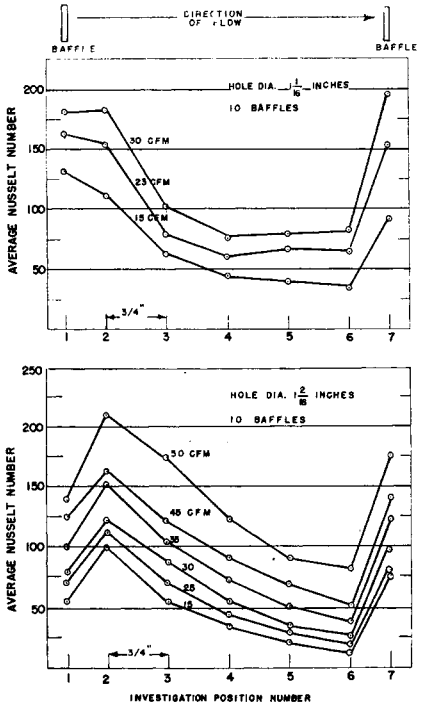

Fig. 6. Variation of Nusselt number along tube.

coming thicker as the distance from the upstream baffle increases.

Zone C, by definition, is the zone where the local Nusselt number assumes a constant minimum value. Over the entire length of this zone the boundary layer maintains a more or less constant thickness, and entrance effects of the baffle have disappeared. Zone C is not apparent in the case of 4.0-in. baffle spacing; that is the Nusselt number decreases steadily and reaches a minimum immediately before the downstream baffle (Figure 6). With 9.0-in spacing Zone C extends about 4.5 in. in all cases. From these results it would appear that Zone C

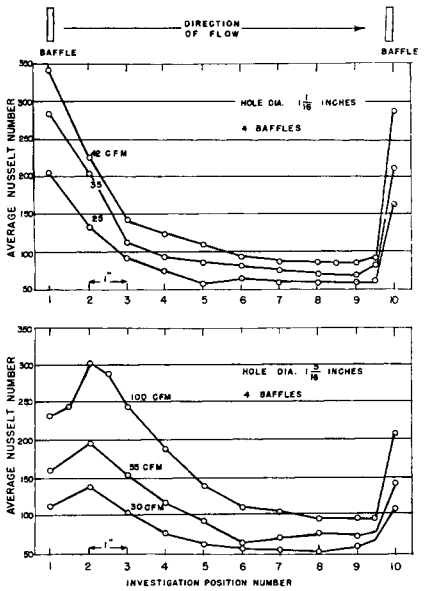

Fig. 7. Variation of Nusselt number along tube.

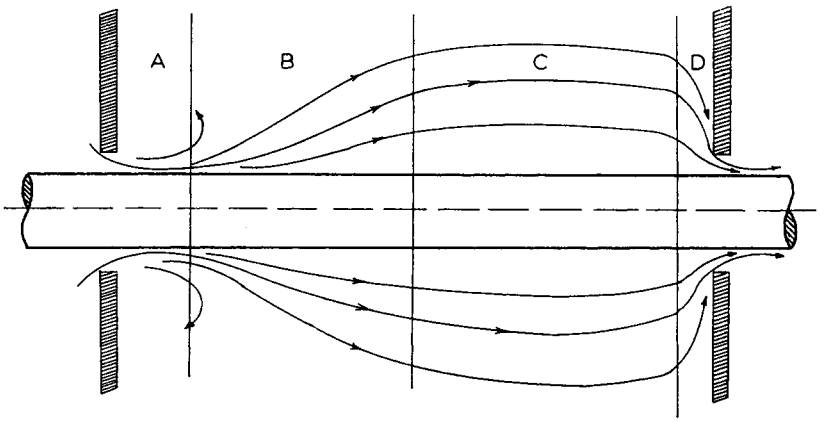

Fig. 8. Flow pattern.

would not exist for any baffle spacing less than 4 in.; that is the effect of the upstream baffle extends to about 4 to 4.5 in. downstream in all cases

Zone D is adjacent to the downstream baffle and is characterized by a rapidly increasing heat transfer rate due to the sudden restriction on the flow area rendered by the downstream baffle. Its length is constant at a value of 0.5 in. in all cases. From the foregoing analysis a schematic sketch of flow paths in the various flow zones is presented in Figure 8.

An increase in baffle spacing from 4.0 to 9.0 in. caused the average heat transfer rate to decrease by approximately 30%. However as pointed out earlier the heat transfer rate at the baffles was not affected by the baffle spacings. The over-all decrease in the average heat transfer rate with an increase in baffle spacing is mainly due to the extension of the lower heat transfer zone (Zone C, Figure 8) as the distance between two adjacent baffles becomes greater. Studies are required at small baffle spacings to determine to what extent the high heat transfer Zones A and B may be utilized in increasing the over-all heat transfer rate in the heat exchanger.

Variations in the Heat Transfer Rate Around the Tube

The variation in the local heat transfer coefficient around the tube was expressed as the ratio of the local heat transfer coefficient to the average coefficient at a given cross section. The data with run numbers 151 and 153 are presented in Table 4 as an example of the minimum and maximum variation detected around the tube. In most cases variations in the local heat transfer coefficient around the tube was less than ± 10% of the average coefficient, indicating that flow in general is parallel to the tube as expected. Since flow was parallel to the tube, there should have been little circumferential variation of the local coefficient. The variation that did occur probably was caused by slight eccentricity of the tubes in the baffle hole and also by the presence of neighboring surfaces (tubes and shell).

Analysis of Pressure-Drop Data

The pressure drop on the shell side of the heat exchanger is composed of losses resulting from enlargement and contraction losses at the inlet and outlet of the exchanger, skin friction from flow parallel to the tube and the shell, and flow through the clearances at the baffles.

In order to calculate the pressure drop across a single baffle from the pressure drop across the whole exchanger the first two items were partially eliminated by subtracting from the over-all pressure drop with baffles the pressure drop without baffles. The difference was divided by the number of baffles in the heat exchanger to obtain the pressure drop across a single baffle; that is

$$\text{Pressure drop across a single baffle} = \frac{\text{Over-all pressure drop with baffles} - \text{Pressure drop without baffles}}{\text{(Number of baffles)}} \qquad (7)$$

The discharge coefficient for the annular opening between tube and baffle was calculated from the following equation:

$$V_b = C\sqrt{\frac{2g_c(\Delta p)_b}{\rho}} \qquad (8)$$

The linear velocity through the baffle openings was calculated by dividing the flow rate by the net flow area at the baffle. The pressure drop across a single baffle was calculated in accordance with Equation (7). In Figure 9 the discharge coefficient calculated from Equation (8) is plotted vs. the equivalent Reynolds number at the baffle (D_eG_b/μ). The discharge coefficients obtained for the 9.0-in. baffle

Table 4. Variations in Local Heat Transfer Coefficients Around the Tube

Run No.	h_1/h_{av}	h_2/h_{av}	h_3/h_{av}	h_4/h_{av}	h_5/h_{av}	h_6/h_{av}	h_7/h_{av}
151	0.930	0.8836	0.934	0.934	1.044	1.157	1.112
153	1.033	0.9910	1.015	1.073	0.975	0.961	0.949

Table 5. Prediction of Local Nusselt Numbers at Segmental Baffles

No. of tubes	No. of baffles	Flow rate, (cu. ft./min.) (60°F., 1 atm.)	Pressure drop, $(\Delta p)_b$ (lb./sq. ft.)	Predicted, $(Nu)_b$	Experimental,* $(Nu)_b$
		Ambrose's Data			
14	2	60	9.50	165	108.15
14	4	60	5.58	141	117.00
14	6	60	4.10	117	130.86
14	10	60	3.22	105	153.65
4	2	60	2.86	99	113.86
4	4	60	2.24	89	129.30
4	6	60	1.99	85	136.40
4	10	60	2.00	85	158.92
		Gurushankariah's data			
14	6	60	4.55	125	131.04
14	6	90	10.10	168	177.17
14	6	120	17.65	206	208.55
14	10	60	3.60	110	124.02
14	10	90	8.06	154	166.36
14	10	120	14.15	190	199.60

* Based on the baffle-to-tube clearance of $\frac{1}{32}$ in.

spacing were generally lower than those for the 4.0-in. spacing. The data are compared with those of Sullivan and Bergelin (9) who used a petroleum oil. The agreement between Sullivan's data and the present data was good for Reynolds numbers greater than 3,000.

An alternate method of presenting pressure-drop data was adopted from Sullivan and Bergelin (9) by the use of an orifice-pressure-drop function defined as

$$\phi = \frac{2g_0 \rho D_e^2 (\Delta p)_b}{\mu^2} \qquad (9)$$

In Figure 10 ϕ is plotted vs. $(D_e/G_b/\mu)$, and all data lie close to a single line with an approximate slope of 2.0. The data of Sullivan and Bergelin are represented by the broken line. Agreement between the two sets is good at high Reynolds numbers.

Prediction of Nusselt Number at the Baffles for the Segmental Baffles

The correlation in Figure 10 enables one to calculate the amount of flow through the annular clearances between a baffle and tubes if the baffle pressure drop is known. From Equation (6) the local heat transfer coefficients at the baffle may be predicted.

The character of flow in segmentally baffled heat exchangers is much different than in orifice baffled heat exchangers. However at the annular clearance between the tube and the baffle some similarity exists between the two types of heat exchangers. On this basis the results of Equation (6) and Figure 10 are used to predict $(N_{Nu})_b$ for the segmental baffles that were investigated by Ambrose (2) and Gurushankariah (4). The results are shown in Table 5.

The pressure drop across a segmental baffle was estimated by dividing the overall pressure drop reported by these workers by the number of baffles, that is $(\Delta p)_T/N$. Actually the pressure difference across a segmental baffle is not a fixed value as calculated above, but rather it de-

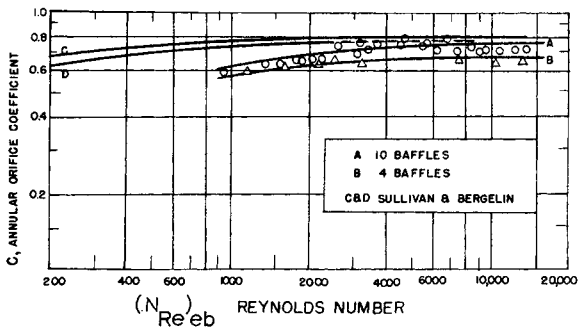

Fig. 9. Annular orifice coefficient vs. Reynolds number.

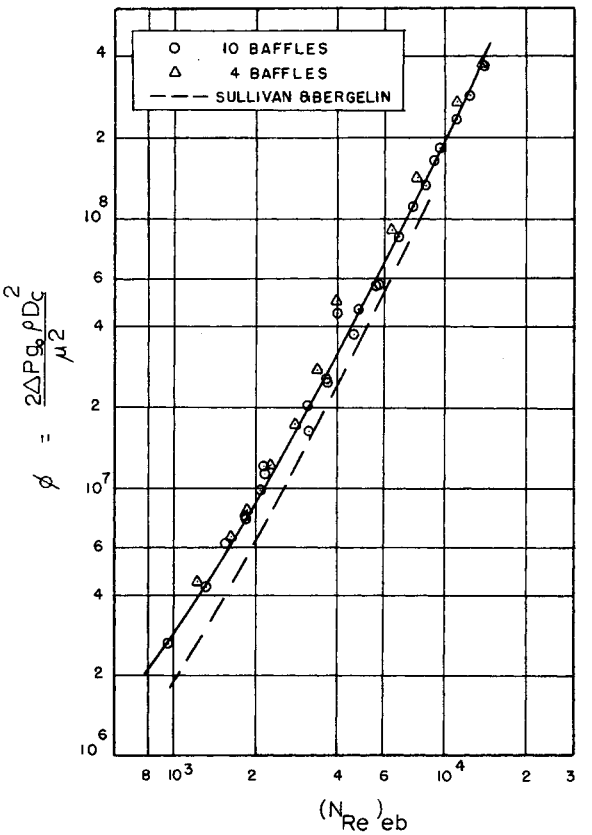

Fig. 10. Orifice pressure-drop function vs. Reynolds number.

creases from a maximum at the root of the baffle to a minimum at the baffle cut. Therefore the pressure drop $(\Delta p)_b$ evaluated here is only a first approximation. For each $(\Delta p)_b$ thus estimated the equivalent Reynolds number $(D_e G_b/\mu)$ was determined from Figure 10, which was then substituted into Equation (6) to obtain the average local Nusselt number at the baffle position.

The experimental value of $(N_{Nu})_b$ in Table 5 is the arithmetic average of all the local Nusselt numbers at the baffle. The agreement is fairly good for the six- and ten-baffle exchangers with fourteen tubes. Other cases show relatively poor agreement.

The pressure drop per baffle $(\Delta p)_b$ is not equal to the true pressure drop across the annular orifice. There will be some recovery of this pressure drop downstream from the orifice, and $(\Delta p)_b$ represents the net pressure loss per baffle. The poor agreement in Table 5 may be due to the use of net pressure loss rather than true pressure loss in predicting the heat transfer rate at the baffle. The amount of pressure recovery is a function of the tube spacing and size of orifice, and these should be considered in the correlation. Further studies to determine the pressure profile along the tube in the vicinity of the baffle will allow a more thorough understanding of the flow processes at the baffle.

CONCLUSIONS

The shell side heat transfer data for a model heat exchanger with orifice baffles were correlated with an empirical equation:

$$\left(\frac{h_s D_1}{k}\right)_{av}\left(\frac{c_p\mu}{k}\right)^{-1/3} = 0.1625\left(\frac{L}{S}\right)^{0.35}\left(\frac{D_1 G_e}{\mu}\right)^{0.67} \quad (4)$$

The exponent on L/S was determined for only two baffle spacings and needs to be checked with further work.

The average value of local heat transfer coefficients at an annular clearance formed between an orifice baffle and a tube were correlated with an empirical equation:

$$\left(\frac{h_s D_1}{k}\right)_{b}\left(\frac{c_p\mu}{k}\right)^{-1/3} = 0.2388\left(\frac{D_1}{D_e}\right)^{0.57}\left(\frac{D_e G_b}{\mu}\right)^{0.67} \quad (6)$$

At a given flow rate an increase in the baffle-to-tube clearance resulted in a decrease in heat transfer rate.

A decrease in baffle spacing for a given length of an exchanger at a given flow rate caused an increase in the heat transfer rate. A decrease in the baffle spacing from 9.0 to 4.0 in. increased the heat transfer rate by as much as 30%.

Four flow zones between the baffles are postulated from the analysis of the Nusselt number distribution along the tube length.

The local heat transfer coefficients around a tube are fairly constant at a given tube cross section. Variations in the local coefficient around the tube were generally of the order of ± 10% of the average coefficient.

An annular orifice coefficient of discharge was defined and used for the analysis of the pressure-drop data. The discharge coefficient was correlated with an equivalent Reynolds number at the baffle. An orifice-pressure-drop function was defined after the manner of Sullivan and Bergelin (9). The function was plotted vs. the equivalent Reynolds number. The present data compared well with the data of other investigators. The plot enables one to calculate the amount of flow through the annular area formed between a baffle and a tube if the pressure drop across the baffle is known or can be estimate, but more detailed data on the pressure distribution at the baffle are necessary.

ACKNOWLEDGMENT

Appreciation is expressed to the National Science Foundation for a grant to support this research.

NOTATION

A_a = annular area between a baffle hole and tube, sq. ft.
A_b = flow area available at the baffle, sq. ft.
A_f = flow area in the region between the baffle, sq. ft.
A_e = geometric mean area $(= \sqrt{A_b A_f})$, sq. ft.
C = annular discharge coefficient
c_p = heat capacity of the fluid, B.t.u./(lb.)(°F.)
D_1 = outside diameter of the tube, ft.
D_2 = baffle hole diameter, ft.
D_e = diameter, twice the clearance between the tube and baffle
D_s = shell diameter, ft.
g_o = gravitational constant
G_b = mass velocity at the baffle, lb./(sq.ft.)(hr.)
G_f = mass velocity in region between baffles, lb./(sq.ft.)(hr.)
G_e = geometric mean mass velocity $(= \sqrt{G_f G_b})$, lb./(sq.ft.)(hr.)
G_x = effective mass velocity [defined by Equation (5)], lb./(sq.ft.)(hr.)
h_s = shell side heat transfer coefficient, B.t.u./(hr.)(sq.ft.)(°F.)
i = electric current, amp.
k = thermal conductivity, B.t.u./(hr.)(sq.ft.)(°F./ft.)
L = effective length of exchanger, ft.
N = number of baffles
P = tube pitch, ft.
$(\Delta p)_b$ = pressure drop across a single baffle, lb./sq.ft.
$(\Delta p)_T$ = over-all shell side pressure drop, lb./sq.ft.
S = baffle spacing, ft.
t = temperature of resistance ribbon, °F.
t_a = temperature of fluid °F.
V_b = fluid velocity through baffle holes, ft./hr.
θ = angle measured from leading edge of a tube, deg.
μ = viscosity, lb./(ft.)(hr.)
ρ = density of fluid, (lb./cu.ft.)

Dimensionless groups

$(N_{Nu})_{av}$ = average Nusselt number, $(h_s D_1/k)_{av}$
$(N_{Nu})_b$ = Nusselt number at baffle, $(h_s D_1/k)_b$
N_{Pr} = Prandtl number, $(c_p\mu/k)$
$(N_{Re})_e$ = geometric mean Reynolds number, $(D_1 G_e/\mu)$
$(N_{Re})_{eb}$ = equivalent Reynolds number at baffle, $(D_e G_b/\mu)$
$(N_{Re})_x$ = effective Reynolds number, $(D_1 G_x/\mu)$
ϕ = orifice-pressure-drop function, $(2g_o\rho(\Delta p)_b D_e^2/\mu^2)$

LITERATURE CITED

1. Ambrose, T. W., Ph.D. thesis, Oregon State College, Corvallis, Oregon (1957).
2. ———, and J. G. Knudsen, *A.I.Ch.E. Journal*, **4**, 332 (1958).
3. Donohue, Daniel A., *Ind. Eng. Chem.*, **41**, 2499 (1949).
4. Gurushankariah, Mysore S., and J. G. Knudsen, *Chem. Eng. Progr. Symposium Ser. No. 29*, **55**, 29 (1959).
5. Lee, Kyu S., M.S. thesis, Oregon State College, Corvallis, Oregon (1959).
6. Milne, William E., "Numerical Calculus," p. 96, Princeton Univ. Press, Princeton, New Jersey (1949).
7. Rubesin, M. W., *Natl. Advisory Comm. Aeronaut., Tech. Note 2345* (1951).
8. Short, B. E., *Trans. Am. Soc. Mech. Engrs.*, **64**, 780 (1942).
9. Sullivan, F. W., and O. P. Bergelin, *Chem. Eng. Progr. Symposium Ser. No. 52*, **18**, 85 (1956).
10. Tinker, Townsend, "Proceedings of the General Discussions on Heat Transfer," *Inst Mech. Engrs., Am. Soc. Mech. Engrs.*, p. 89 (1952).

Manuscript received July 28, 1959; revision received March 18, 1960; paper accepted March 21, 1960. Paper presented at A.I.Ch.E. San Francisco meeting.